arXiv:1606.05907v2 [stat.AP] 2 Feb 2017

# Spectral model selection in the electronic measurement of the Boltzmann constant by Johnson noise thermometry

**Kevin J Coakley**[1], **Jifeng Qu**[2]

[1] National Institute of Standards and Technology (NIST), Boulder, CO 80302 USA
[2] National Institute of Metrology (NIM), Beijing 100029, Peoples Republic of China

E-mail: kevin.coakley@nist.gov

## 1. Abstract

In the electronic measurement of the Boltzmann constant based on Johnson noise thermometry, the ratio of the power spectral densities of thermal noise across a resistor at the triple point of water, and pseudo-random noise synthetically generated by a quantum-accurate voltage-noise source is constant to within 1 part in a billion for frequencies up to 1 GHz. Given knowledge of this ratio, and the values of other parameters that are known or measured, one can determine the Boltzmann constant. Due, in part, to mismatch between transmission lines, the experimental ratio spectrum varies with frequency. We model this spectrum as an even polynomial function of frequency where the constant term in the polynomial determines the Boltzmann constant. When determining this constant (offset) from experimental data, the assumed complexity of the ratio spectrum model and the maximum frequency analyzed (fitting bandwidth) dramatically affects results. Here, we select the complexity of the model by cross-validation – a data-driven statistical learning method. For each of many fitting bandwidths, we determine the component of uncertainty of the offset term that accounts for random and systematic effects associated with imperfect knowledge of model complexity. We select the fitting bandwidth that minimizes this uncertainty. In the most recent measurement of the Boltzmann constant, results were determined, in part, by application of an earlier version of the method described here. Here, we extend the earlier analysis by considering a broader range of fitting bandwidths and quantify an additional component of uncertainty that accounts for imperfect performance of our fitting bandwidth selection method. For idealized simulated data with additive noise similar to experimental data, our method correctly selects the true complexity of the ratio spectrum model for all cases considered. A new analysis of data from the recent experiment yields evidence for a temporal trend in the offset parameters.

Keywords: Boltzmann constant, cross-validation, Johnson noise thermometry, model selection, resampling methods, impedance mismatch

## 2. Introduction

There are various experimental methods to determine the Boltzmann constant including acoustic gas thermometry [1],[2],[3]; dielectric constant gas thermometry [4],[5], [6], [7], Johnson noise thermometry

(JNT) [8], [9], [10], and Doppler broadening [11], [12]. CODATA (Committee on Data for Science and Technology) will determine the Boltzmann constant as a weighted average of estimates determined with these methods. Here, we focus on JNT experiments which utilize a quantum-accurate voltage-noise source (QVNS).

In JNT, one infers true thermodynamic temperature based on measurements of the fluctuating voltage and current noise caused by the random thermal motion of electrons in all conductors. According to the Nyquist law, the mean square of the fluctuating voltage noise for frequencies below 1 GHz and temperature near 300 K can be approximated to better than 1 part in billion as $< V^2 >= 4kTR\Delta f$, where $k$ is the Boltzmann constant, $T$ is the thermodynamic temperature, $R$ is the resistance of the sensor, and $\Delta f$ is the bandwidth over which the noise is measured. Since JNT is a pure electronic measurement that is immune from chemical and mechanical changes in the material properties of the sensor, it is an appealing alternative to other forms of primary gas thermometry that are limited by the non-ideal properties of real gases.

Recently, interest in JNT has dramatically increased because of its potential contribution to the "New SI" (New International System), in which the unit of thermodynamic temperature, the kelvin, will be redefined in 2018 by fixing the numerical value of $k$. Although almost certainly the value of $k$ will be primarily determined by the values obtained by acoustic gas thermometry, there remains the possibility of unknown systematic effects that might bias the results, and therefore an alternative determination using a different physical technique and different principles is necessary to ensure that any systematic effects must be small. To redefine the kelvin, the Consultative Committee on Thermometry (CCT) of the International Committee for Weights and Measures (CIPM) has required that besides the acoustic gas thermometry method, there must be another method that can determine $k$ with a relative uncertainty below $3\times10^{-6}$. As of now, JNT is the most likely method to meet this requirement.

In JNT with a QVNS, [10], according to physical theory, the Boltzmann constant is related to the ratio of the power spectral density (PSD) of noise produced by a resistor at the triple point of water temperature and the PSD of noise produced by a QVNS. For, frequencies below 1 GHz, this ratio is constant to within 1 part in $10^9$. The physical model for the PSD for the noise across the resistor is $S_{\rm R}$ where

$$S_{\rm R} = 4kT_{\rm W}X_{\rm R}R, \tag{1}$$

$T_{\rm W}$ is the temperature of the triple point of water, $X_{\rm R}$ is the resistance in units of the von Klitzing resistance $R_{\rm K} = \frac{h}{e^2}$ where $e$ is the charge of the electron and $h$ is Planck's constant. The model for the PSD of the noise produced by the QVNS, $S_{\rm Q}$, is

$$S_{\rm Q} = D^2N_{\rm J}^2f_{\rm s}M/K_{\rm J}^2, \tag{2}$$

where $K_{\rm J} = \frac{2e}{h}$, $f_{\rm s}$ is a clock frequency, $M$ is a bit length parameter, $D$ is a software input parameter that determines the amplitude of the QVNS waveform, and $N_{\rm J}$ is the number of junctions in the Josephson array in the QVNS. Assuming that the Eq. 1 and Eq. 2 models are valid, the Boltzmann constant $k$ is

$$k = h\frac{DN_{\rm J}^2f_{\rm s}M}{16T_{\rm W}X_{\rm R}}\frac{S_{\rm R}}{S_{\rm Q}}. \tag{3}$$

In actual experiments, transmission lines that connect the resistor and the QVNS to preamplifiers produce a ratio spectrum that varies with frequency. Due solely to impedance mismatch effects, for the frequencies

of interest, one expects the ratio spectrum predicted by physical theory to be an even polynomial function of frequency where the constant term (offset) in the polynomial is the value $S_{\mathrm{R}}/S_{\mathrm{Q}}$ provided that dielectric losses are negligible. The theoretical justification for this polynomial model is based on low-frequency filter theory where measurements are modeled by a "lumped-parameter approximation." In particular, one models the networks for the resistor and the QVNS as combination of series and parallel complex impedances where the impedance coupling in the resistor network is somewhat different from that in the QVNS network. For the ideal case where all shunt capacitive impedances are real, there are no dielectric losses. As a caveat, in actual experiments, other effects including electromagnetic interference and filtering aliasing also affect the ratio spectrum. As discussed in [10], for the the recent experiment of interest, dielectric losses and other effects are small compared to impedance mismatch effects. As an aside, impedance mismatch effects also influence results in JNT experiments that do not utilize a QVNS [13], [14], [15].

Based on a fit of the ratio spectrum model to the observed ratio spectrum, one determines the offset parameter $S_{\mathrm{R}}/S_{\mathrm{Q}}$. Given this estimate of $S_{\mathrm{R}}/S_{\mathrm{Q}}$ and values of other terms on the right hand sided of Eq. 3 (which are known or measured), one determines the Boltzmann constant. However, the choice of the order $d$ (complexity) of the polynomial ratio spectrum model and the upper frequency cutoff for analysis (fitting bandwidth $f_{\mathrm{max}}$) significantly affects both the estimate and its associated uncertainty. In JNT, researchers typically select the model complexity and fitting bandwidth based on scientific judgement informed by graphical analysis of results. A common approach is to restrict attention to sufficiently low fitting bandwidths where curvature in the ratio spectrum is not too dramatic and assume that a quadratic spectrum model is valid (see [9] for an example of this approach).

In contrast to a practitioner-dependent subjective approach, we present a data-driven objective method to select the complexity of the ratio spectrum model and the fitting bandwidth. In particular, we select the ratio spectrum model based on cross-validation [19],[20],[21],[22]. We note that in addition to cross-validation, there are other model selection methods including those based on the Akaike Information Criterion (AIC) [16], the Bayesian Information Criterion (BIC) [17], $C_p$ statistics [18]. However, cross-validation is more data-driven and flexible than these other approaches because it relies on fewer modeling assumptions. Since the selected model determined by any method is a function of random data, none perform perfectly. Hence, uncertainty due to imperfect model selection performance should be accounted for in the uncertainty budget for any parameter of interest [23], [24]. Failure to account for uncertainty in the selected model generally leads to underestimation of uncertainty.

In cross-validation, one splits observed data into training and validation subsets. One fits candidate models to training data, and selects the model that is most consistent with validation data that are independent of the training data. Here (and in most studies) consistency is measured with a cross-validation statistic equal to the mean square deviation between predicted and observed values in validation data. We stress that, in general, this mean square deviation depends on both random and systematic effects.

For each candidate model, practitioners sometimes average cross-validation statistics from many random splits of the data into training and validation data set [25], [26], [27]. Here, from many random splits, we instead determine model selection fractions determined from a five-fold cross-validation analysis. Based on these model selection fractions, we determine the uncertainty of the offset parameter for each fitting bandwidth of interest. We select $f_{\mathrm{max}}$ by minimizing this uncertainty. As far as we know, our resampling approach for

quantification of uncertainty due to random effects and imperfect performance of model selected by five-fold cross-validation is new. As an aside, for the case where models are selected based on $C_p$ statistics, Efron [28] determined model selection fractions with a bootstrap resampling scheme.

In [10], the complexity of the ratio spectrum and the fitting bandwidth were selected with an earlier version of the method described here for the case where $f_{\text{max}}$ was no greater than 600 kHz. Here, we re-analyze the data from [10] but allow $f_{\text{max}}$ to be as large as 1400 kHz. In this work, we also quantify an additional component of uncertainty that accounts for imperfect performance of our method for selecting the fitting bandwidth. We stress that this work focuses only on the uncertainty of the offset parameter in ratio spectrum model. For a discussion of other sources of uncertainty that affect the estimate of the Boltzmann constant, see [10]. In a simulation study, we show that our methods correctly selects the correct ratio spectrum for simulated data with additive noise similar to observed data. Finally, for experimental data, we quantify evidence for a possible linear temporal trend in estimates for the offset parameter.

## 3. Methods

### *3.1. Physical model*

Following [10], to account for impedance mismatch effects, we model the ratio of the power spectral densities of resistor noise and QVNS noise, $r_{\text{model}}(f)$, as a $d$th order even polynomial function of frequency as follows

$$r_{\text{model}}(f) = \sum_{i=0}^{i_{\text{max}}} \alpha_{2j} (\frac{f}{f_0})^{2i}, \tag{4}$$

where $d = 2i_{\text{max}}$, and $f_0$ is a reference frequency (1 MHz in this work). Throughout this work, as shorthand, we refer to this model as a $d = 2$ model if $i_{\text{max}} = 1$, a $d = 4$ model if $i_{\text{max}} = 2$, and so on. The constant term, $a_0$ in the Eq. 4 model corresponds to $S_{\text{R}}/S_{\text{Q}}$ where $S_{\text{R}}$ and $S_{\text{Q}}$ are predicted by Eq. 1 and Eq 2. respectively.

### *3.2. Experimental data*

Data was acquired for each of 45 runs of the experiment [10]. Each run occurred on a distinct day between June 12, 2014 to September 10, 2014. The time to acquire data for each run varied from 15 h to 20 h. For each run, Fourier transforms of time series corresponding to the resistor at the triple point of water temperature and the QVNS were determined at a resolution of 1 Hz for frequencies up to 2 MHz. Estimates of mean PSD were formed for frequency blocks of width 1.8 kHz. For the frequency block with midpoint $f$, for the $i$th run, we denote the mean PSD estimate for the resistor noise and QVNS noise for the $i$th run as $S_{\text{R,obs}}(f, i)$ and $S_{\text{Q,obs}}(f, i)$ respectively where $i = 1,2, \cdots 45$.

Following [10], we define a reference value $a_{0,\text{calc}}$ for the offset term in our Eq. 4 model as

$$a_{0,\text{calc}} = \frac{4k_{2010}RT}{S_{\text{Q,calc}}}, \tag{5}$$

where $k_{2010}$ is the CODATA2010 recommended value of the Boltzmann constant, $R$ is the measured resistance of the resistor with traceability to the quantum Hall resistance, $T$ is the triple point water temperature and $S_{\text{Q,calc}}$ is the calculated power spectral density of QVNS noise.

In the recent experiment the true value of the resistance, $R$, could have varied from run-to-run. Hence, in [10], $R$ was measured for each run in a calibration experiment. Based on these calibration experiments, $a_{0,\text{calc}}$ was determined for each run. The difference between the maximum and minimum of the estimates determined from all 45 runs is 2.36 $\times 10^{-6}$. For the $i$th run, we denote the values $a_0$ and $a_{0,\text{calc}}$ as $a_0(i)$ and $a_{0,\text{calc}}(i)$ respectively. Even though $a_0(i)$ and $a_{0,\text{calc}}(i)$ vary from run-to-run, we assume that temporal variation of their difference, $a_0(i) - a_{0,\text{calc}}(i)$, is negligible. Later in this work, we check the validity of this key modeling assumption. The component of uncertainty of the estimate of $a_{0,\text{calc}}$ for any run due to imperfect knowledge of $R$ is approximately 2 $\times 10^{-7}$. The estimated weighted mean value of our estimates, $\hat{\bar{a}}_{0,\text{calc}}$, is 1.000100961. The weights are determined from relative data acquisition times for the runs.

Following [10], for each frequency, we pool data from all 45 runs to form a numerator term $\sum_{i=1}^{45} S_{\text{R,obs}}(f,i)$ and a denominator term $\sum_{i=1}^{45} S_{\text{Q,obs}}(f,i)$. From these two terms, we estimate one ratio for each frequency as

$$r_{\text{obs}}(f) = \frac{\sum_{i=1}^{45} S_{\text{R,obs}}(f,i)}{\sum_{i=1}^{45} S_{\text{Q,obs}}(f,i)} \tag{6}$$

(see Figure 1). From the Eq. 6 ratio spectrum, we estimate one residual offset term $a_0 - \bar{a}_{0,\text{calc}}$ where $\bar{a}_{0,\text{calc}}$ is the weighted mean of $a_{0,\text{calc}}$ values from all runs.

### *3.3. Model selection method*

In our cross-validation approach, we select the model that produces the prediction (determined from the training data) that is most consistent with the validation data. Since $a_{0,\text{calc}}$ varies from run-to-run, we correct $S_{\text{R,obs}}$ spectra so that our cross-validation statistic is not artificially inflated by run-to-run variations in $a_{0,\text{calc}}$. The corrected ratio spectrum for the $i$th run is

$$r_{\text{cor}}(f) = \frac{\sum_{i=1}^{45} S_{\text{R,cor}}(f,i)}{\sum_{i=1}^{45} S_{\text{Q,obs}}(f,i)} \tag{7}$$

where

$$S_{\text{R,cor}}(f,i) = S_{\text{R,obs}}(f,i) - (\hat{a}_{0,\text{calc}}(i) - \hat{\bar{a}}_{0,\text{calc}}) S_{\text{Q,obs}}(f,i). \tag{8}$$

In effect, given that our calibration experiment measurement of $a_{0,\text{calc}}(i)$ has negligible systematic error, the above correction returns produces a spectrum where the values of $a_0$ should be nearly the same for all runs. We stress that after selecting the model based on cross-validation analysis of corrected spectra (see Eq. 7), we estimate $a_0 - \bar{a}_{0,\text{calc}}$ from the uncorrected Eq. 6 spectrum.

In our cross-validation method, we generate 20 000 random five-way splits of the data. In each five-way split, we assign the pair of spectra, ($S_{\text{R,cor}}$ and $S_{\text{Q,obs}}$), from any particular run to one of the five subsets by a resampling method. Each of the 45 spectral pairs appears in one and only one of the five subsets. We resample spectra according to run to retain possible correlation structure within the spectrum for any particular run. Each simulated five-way split is determined by a random permutation of the positive integers from 1 to 45. The first nine permuted integers corresponds to the runs assigned to the first subset. The second nine correspond to the runs assigned to the second subset, and so on. From each random split, four of the subsets are aggregated to form training data, and the other subset forms the validation data. Within the training data, we pool all

$S_{\text{R,cor}}$ spectrum and all $S_{\text{Q,obs}}$ spectrum and form one ratio spectrum. Similarly, for the validation data, we pool all $S_{\text{R,obs}}$ spectrum and $S_{\text{Q,obs}}$ spectrum and form one ratio spectrum. We fit each candidate polynomial ratio spectrum model to the training data, and predict the observed ratio spectrum in the validation data based on this fit. We then compute the (empirical) mean squared deviation (MSD) between predicted and observed ratios for the validation data. For any random five-way split, there are five ways of defining the validation. Hence, we compute five MSD values for each random split. The cross-validation statistic for each $d$, CV($d$), is the average of these five MSD values. For each random five-way split, we select the model that yields the smallest value of CV($d$). Based on 20 000 random splits of the 45 spectra, we estimate a probability mass function $\hat{p}(d)$ where the possible values of $d$ are: 2,4,6,8,10,12 or 14.

### *3.4. Uncertainty quantification*

For any choice of $f_{\text{max}}$, suppose that $d$ is known exactly. For this ideal case, based on a fit of the ratio spectrum model to the Eq. 6 ratio spectrum, we could construct a coverage interval for $a_0$ with standard asymptotic methods or with a parametric bootstrap method [29]. For our application, we approximate the parametric bootstrap distribution of our estimate of $a_0$ as a Gaussian distribution with mean $\hat{a}_0$ and variance $\hat{\sigma}^2_{\hat{a_0}(d),\text{ran}}$, where $\hat{\sigma}_{\hat{a_0}(d),\text{ran}}$ is predicted by asymptotic theory. To account for the effect of uncertainty in $d$ on our estimate of $a_0$, we form a mixture of bootstrap distributions as follows

$$f(x) = \sum_d \hat{p}(d) g(x, \hat{a}_0(d), \hat{\sigma}^2_{\hat{a_0}(d),\text{ran}}), \tag{9}$$

where $g(x, \mu, \sigma^2)$ is the probability density function (pdf) for a Gaussian random variable with expected value $\mu$ and variance $\sigma^2$. For any $f_{\text{max}}$, we select the $d$ that yields the largest value of $\hat{p}(d)$. Given that the probability density function (pdf) of a random variable $X$ is $f(x) = \sum_{i=1}^{n} w_i f_i(x)$, and the mean and variance of a random variable $Z$ with pdf $f_i(z)$ are $\mu_i$ and $\sigma_i^2$, the mean and variance of $X$ are

$$E(X) = \mu = \sum_{i=1}^{n} w_i \mu_i, \tag{10}$$

and

$$VAR(X) = \sum_{i=1}^{n} w_i \sigma_i^2 + \sum_{i=1}^{n} w_i (\mu_i - \mu)^2. \tag{11}$$

Hence, the mean and variance of a random variable sampled from the Eq. 9 pdf are $\hat{\bar{a}}_0$ and $\hat{\sigma}^2_{\text{tot}}$ respectively, where

$$\hat{\bar{a}}_0 = \sum_d \hat{p}(d) \hat{a}_0(d), \tag{12}$$

and

$$\hat{\sigma}^2_{\text{tot}} = \tilde{\sigma}^2_\alpha + \tilde{\sigma}^2_\beta, \tag{13}$$

where

$$\tilde{\sigma}^2_\alpha = \sum_d \hat{p}(d) \hat{\sigma}^2_{\hat{a}_0(d),\text{ran}}, \tag{14}$$

and

$$\tilde{\sigma}_\beta^2 = \sum_d \hat{p}(d)(\hat{a}_0(d) - \hat{\bar{a}}_0)^2. \tag{15}$$

For each $f_{\max}$ value, we estimate the uncertainty of our estimate of $a_0$ as $\hat{\sigma}_{\text{tot}}$. We select $f_{\max}$ by minimizing $\hat{\sigma}_{\text{tot}}$ on grid in frequency space. For any fitting bandwidth, $\tilde{\sigma}_\beta$ is the weighted-mean-square deviation of the estimates of $a_0$ from the candidate models about their weighted mean value where the weights are the empirically determined selection fractions. The term $\tilde{\sigma}_\alpha$ is the weighted variance of the parametric bootstrap sampling distributions for the candidate models where the weights are again the empirically determined selection fractions. We stress that both $\tilde{\sigma}_\alpha$ and $\tilde{\sigma}_\beta$ are affected by imperfect knowledge of the ratio spectrum model.

## 4. Results

### *4.1. Analysis of Experimental data*

We fit candidate ratio spectrum models to the Eq. 6 observed ratio spectrum by the method of Least Squares (LS). We determine model selection fractions (Table 1) and $\hat{\sigma}_{\text{tot}}$ (Table 2) for $f_{\max}$ values on an evenly space grid (with spacing of 25 kHz) between 200 kHz and 1400 kHz. In Figure 2, we show how selected $d$, $\hat{\sigma}_{\text{tot}}$ and $\hat{a}_0 - \hat{\bar{a}}_{0,\text{calc}}$ vary with $f_{\max}$. Our method selects $(f_{\max}, d)$ = ( 1250 kHz, 8), $\hat{\sigma}_{\text{tot},*} = 3.25 \times 10^{-6}$, and $\hat{a}_0 - \hat{\bar{a}}_{0,\text{calc}} = 2.36 \times 10^{-6}$. In Figure 3, we show results for the values of $f_{\max}$ ( that yield the five lowest values of $\hat{\sigma}_{\text{tot}}$. For these five fitting bandwidths (900 kHz, 1150 kHz, 1175 kHz, 1225 kHz and 1250 kHz) $\hat{\sigma}_{\text{tot}}$ values appear to follow no pattern as a function of frequency, however visual inspection suggests that the estimates of $a_0 - \bar{a}_{0,\text{calc}}$ may follow a pattern. It is not clear if the variations in Figure 2 and 3 are due to random or systematic measurement effects. To get some insight into this issue, we study the performance of our method for idealized simulated data that are free of systematic measurement error.

We simulate three realizations of data based on the estimated values of $a_2, a_4, a_6$ and $a_8$ in Table 3. In our simulation, for each run, we set $a_0 - a_{0,\text{calc}} = 0$, $S_{\text{Q,obs}}(f) = 1$ and $S_{\text{R,obs}}(f)$ equals the sum of the predicted ratio spectrum and Gaussian white noise. For each run, the variance of the noise is determined from fitting the ratio spectrum model to the experimental ratio spectrum for that run. For simulated data, the $d$, $\hat{\sigma}_{\text{tot}}$ and $\hat{a}_0 - a_{0,\text{calc}}$ spectra exhibit fluctuations similar to those in the experimental data (Figures 4,5,6). Since variability in simulated data (Figures 4,5,6) is due solely to random effects, we can not rule out the possibility that random effects may have produced the fluctuations in the experimental spectra (Figures 2 and 3). For the third realization of simulated data (Figure 6), the estimated values of $a_0 - a_{0,\text{calc}}$ corresponding to the $f_{\max}$ values that yield the five lowest values of $\hat{\sigma}_{\text{tot}}$ form two clusters in $f_{\max}$ space which are separated by approximately 300 kHz (Figure 7). This pattern is similar to that observed for the experimental data (Figures 3). As a caveat, for the experimental data, we can not rule out the possibility that systematic measurement error could cause or enhance observed fluctuations.

Our method correctly selects the $d$=8 model for each of three independent realizations of simulation data (Table 4). In a second study, we simulate three realizations of data according to a $d$=6 polynomial model based

on the fit to experimental data for $f_{\text{max}} = 900$ kHz. Our methods correctly selects the $d$=6 for each of the three realizations.

In [10], our method selected $f_{\text{max}} = 575$ kHz and $d = 4$ when $f_{\text{max}}$ was constrained to be less than 600 kHz. For these selected values, our current analysis yields $\hat{a}_0 - \hat{\bar{a}}_{0,\text{calc}} = 1.81 \times 10^{-6}$ and $\hat{\sigma}_{\text{tot}} = 3.58 \times 10^{-6}$. In this study, when $f_{\text{max}}$ is allowed to be as large as 1400 kHz, our method selects $f_{\text{max}}$ = 1250 Hz and $d = 8$, and $\hat{a}_0 - \hat{\bar{a}}_{0,\text{calc}} = 2.36 \times 10^{-6}$ and $\hat{\sigma}_{\text{tot},*} = 3.25 \times 10^{-6}$. The difference between the two results, $0.55 \times 10^{-6}$, is small compared to the uncertainty of either result.

We expect imperfections in our fitting bandwidth selection method for various reasons. First, we conduct a grid search with a resolution of 25 kHz rather than a search over a continuum of frequencies. Second, there are surely fluctuations in $\hat{\sigma}_{\text{tot}}$ due to random effects that vary with fitting bandwidth. Third, different values of $f_{\text{max}}$ can yield very similar values of $\hat{\sigma}_{\text{tot}}$ but somewhat different values of $\hat{a}_0 - \hat{\bar{a}}_{0,\text{calc}}$. Therefore, it is reasonable to determine an additional component of uncertainty, $\hat{\sigma}_{f_{\text{max}}}$, that accounts for uncertainty due to imperfect performance of our method to select $f_{\text{max}}$. Here we equate $\hat{\sigma}_{f_{\text{max}}}$ to the estimated standard deviation of estimates of $a_0 - \bar{a}_{0,\text{calc}}$ corresponding to the five $f_{\text{max}}$ values that yielded the lowest $\hat{\sigma}_{\text{tot}}$ values (Figures 3 and 7). For the three realizations of simulated spectra, the corresponding $\hat{\sigma}_{f_{\text{max}}}$ values are $0.39 \times 10^{-6}$, $0.45 \times 10^{-6}$, and $1.83 \times 10^{-6}$. For the experimental data $\hat{\sigma}_{f_{\text{max}}} = 0.56 \times 10^{-6}$. For both simulated and experimental data, our update for the total uncertainty of estimated $a_0$ is $\hat{\sigma}_{\text{tot,final}}$ where

$$\hat{\sigma}_{\text{tot,final}} = \sqrt{\hat{\sigma^2}_{\text{tot},*} + \hat{\sigma^2}_{f_{\text{max}}}}. \tag{16}$$

For the simulated data, $\hat{\sigma}_{\text{tot,final}}$ is $2.69 \times 10^{-6}$, $3.08 \times 10^{-6}$, and $3.42 \times 10^{-6}$. For the experimental data, $\hat{\sigma}_{\text{tot,final}} = 3.29 \times 10^{-6}$. As a caveat, the choice to quantify $\hat{\sigma}_{f_{\text{max}}}$ as the standard deviation of the estimates corresponding to $f_{\text{max}}$ values that yield the five lowest values is based on scientific judgement. For instance, if we determine $\hat{\sigma^2}_{f_{\text{max}}}$ based on the the $f_{\text{max}}$ values that yield the ten lowest rather the five lowest values $\hat{\sigma}_{\text{tot}}$, for the three simulation cases and the observed data we get $\hat{\sigma}_{f_{\text{max}}} = 0.55 \times 10^{-6}$, $1.08 \times 10^{-6}$, $1.42 \times 10^{-6}$, and $0.73 \times 10^{-6}$ respectively.

### *4.2. Stability analysis*

From the corrected Eq.7 spectra, we estimate $a_0 - \bar{a}_{0,\text{calc}}$ for each of the 45 runs by fitting our selected ratio spectrum model ($d = 8$ and $f_{\text{max}} = 1250$ kHz) to the data from each run by the method of LS (Figure 8). Ideally, on average, these estimates should not vary from run-to-run assuming that our Eq. 8 correction model based on calibration data is valid. From these estimates, we determine the slope and intercept parameters for a linear trend model by the method of Weighted Least Squares (WLS) where we minimize

$$\chi^2_{\text{obs}} = \sum_{i=1}^{45} w_i (y_i - \hat{y}_i)^2. \tag{17}$$

Above, for the $i$th run, $y_i$ and $\hat{y}_i$ are the estimated and predicted (according to the trend model) values of $a_0 - \bar{a}_{0,\text{calc}}$, and $w_i$ is the inverse of the squared asymptotic uncertainty of associated with our estimate determined by the LS fit to data from the $i$th run. We determine the uncertainty of the trend model parameters with a nonparametric bootstrap method (see Appendix 1) following [30] (Table 5). We repeat the bootstrap

procedure but set $\hat{y}_i$ to a constant. This analysis yields an estimate of the null distribution of the slope estimate corresponding to the hypothesis that there is no trend. The fraction of bootstrap slope estimates with magnitude greater than or equal to the magnitude of the estimated slope determined from the observed data is the bootstrap $p$-value [29] corresponding to a two-tailed test of the null hypothesis. For the $f_{\text{max}}$ values that yield the five lowest values of $\hat{\sigma}_{tot}$, our bootstrap analysis provides strong evidence that $a_0 - \bar{a}_{0,\text{calc}}$ varies with time. At the value of $f_{\text{max}} = 575$ kHz, there is a moderate amount of evidence for a trend.

For each $f_{\text{max}}$ choice, we test the hypothesis that the linear trend is consistent with observations based on the value of $\chi^2_{\text{obs}}$. If the observed data are consistent with the trend model, a resulting $p$-value from this test is realization of a random variable with a distribution that is approximately uniform between 0 and 1. Hence, the large $p$-values reported column 7 of Table 5 suggest that the asymptotic uncertainties determined by the LS method for each run may be inflated. As a check, we estimate the slope uncertainty with a parametric bootstrap method where we simulate bootstrap replications of the observed data by adding Gaussian noise to the estimated trend with standard deviations equal to the asymptotic uncertainties determined by the LS method. In contrast to the method from [30], the parametric bootstrap method yields larger slope uncertainties. For instance, for the 1250 kHz and 575 kHz cases, the parametric bootstrap slope uncertainty estimates are larger than the corresponding Table 5 estimates by 30 $\%$ and 23 $\%$ respectively. That is, the parametric bootstrap method estimates are inflated with respect to the estimates determined with the method from [30].

This inflation could result due to heteroscedasticity (frequency dependent additive measurement error variances). This follows from the well-known fact that when models are fit to heteroscedastic data, the variance of parameter estimates determined by the LS method are larger than the variance of parameter estimates determined by the ideal WLS method. Based on fits of selected models to data pooled from all runs, we test the hypothesis that the variance of the additive noise in the ratio spectrum is independent of frequency. Based on the Breush-Pagan method [31], the $p$-values corresponding to the test of this hypothesis are 0.723, 0.064, 0.006, 0.001, 0.001 and 0.001 for fitting bandwidths of 575 kHz, 900 kHz, 1150 kHz, 1175 kHz, 1225 kHz, and 1250 kHz respectively. Hence, the evidence for heteroscedasticity is very strong for the larger fitting bandwidths.

For a fitting bandwidth of 1250 kHz, the variation of the estimated trend over the duration of the experiment is $18.2 \times 10^{-6}$. In contrast, the uncertainty of our estimate of $a_0 - \bar{a}_{0,\text{calc}}$ determined under the assumption that there is no trend is only 3.29 $\times 10^{-6}$ (Table 4). The evidence for a linear trend at particular fitting bandwidths above 900 kHz is strong (p-values are 0.012 or less) (column 5 in Table 5). In contrast, the evidence (from hypothesis testing) for a linear trend at 575 kHz (the selected fitting bandwidth in [10]) is not as strong since the p-value is 0.049. However, the larger p-value at 575 kHz may be due to more random variability in the estimated offset parameters rather than lack of a deterministic trend in the offset parameters. This hypothesis is supported by the observation that the uncertainty of the estimated slope parameter due to random effects generally increases as the fitting bandwidth is reduced, and that fact that all of the slope parameter estimates for cases shown in Table 5 are negative and vary from -0.440 $\times 10^{-6}$ / day to -0.164 $\times 10^{-6}$ / day. Together, these observations strongly suggest a deterministic trend in measured offset parameters at a fitting bandwidth of 575 kHz. Currently, experimental efforts are underway to understand the physical source of this (possible) temporal trend.

If there is a linear temporal trend in the offset parameters at a fitting bandwidth of 575 kHz, with slope

similar to what we estimate from data, the reported uncertainty for the Boltzmann constant reported in [10] is optimistic because the trend was not accounted for in the uncertainty budget. To account for the effect of a linear trend on results, one must estimate the associated systematic error due to the trend at some particular time. Unfortunately, we have no empirical method to do this. As a further complication, if there is a trend, it may not be exactly linear.

## 5. Summary

For electronic measurements of the Boltzmann constant by JNT, we presented a data-driven method to select the complexity of a ratio spectrum model with a cross-validation method. For each candidate fitting bandwidth, we quantified the uncertainty of the offset parameter in the spectral ratio model in a way that accounts for random effects as well as systematic effects associated with imperfect knowledge of model complexity. We selected the fitting bandwidth that minimizes this uncertainty. We also quantified an additional component of uncertainty that accounts for imperfect knowledge of the selected fitting bandwidth. With our method, we re-analyzed data from a recent experiment by considering a broader range of fitting bandwidths and found evidence for a temporal linear trend in offset paramaters. For idealized simulated data free of systematic error with additive noise similar to experimental data, our method correctly selected the true complexity of the ratio spectrum model for all cases considered. In the future, we plan to study how well our methods work for other experimental and simulated JNT data sets with variable signal-to-noise ratios and investigate how robust our method is to systematic measurement errors. We expect our method to find broad metrological applications including selection of optimal virial equation models in gas thermometry experiments, and selection of line-width models in Doppler broadening thermometry experiments.

**Acknowledgements.** Contributions of staff from NIST, an agency of the US government, are not subject to copyright in the US. JNT research at NIM is supported by grants NSFC (61372041 and 61001034). Jifeng Qu acknowledges Samuel P. Benz, Alessio Pollarolo, Horst Rogalla, Weston L. Tew of the NIST and Rod White of MSL, New Zealand for their help with the JNT measurements analyzed in this work. We also thank Tim Hesterberg of Google for helpful discussions.

## 6. Appendix 1: nonparametric bootstrap resampling method

We denote the estimate of $a_0 - \bar{a}_{0,\text{calc}}$ from the $i$th run as $y_i$, and the data acquisition time for the $i$th run as $t_i$. Our linear trend model is

$$y = X\beta + \epsilon, \tag{18}$$

where the observed data is $y = (y_1, y_2 \cdots y_{45})^T$, $\epsilon$ is an additive noise term, and the matrix $X$ is

$$\begin{pmatrix} X_{1\,1} & X_{1\,2} \\ X_{2\,1} & X_{2\,2} \\ . & . \\ . & . \\ . & . \\ X_{45\,1} & X_{45\,2} \end{pmatrix} = \begin{pmatrix} 1 & 0 \\ 1 & t_2 - t_1 \\ . & . \\ . & . \\ . & . \\ 1 & t_{45} - t_1 \end{pmatrix},$$

and $\beta = (\beta_0, \beta_1)^T$ where the $\beta_0$ is the intercept parameter and $\beta_1$ is the slope parameter. Above, we model the $i$th component of $\epsilon$ as a realization of a random variable with expected value 0 and variance $\kappa V_i$ where $V_i$ is known but $\kappa$ is unknown. Following [30], the predicted value in a linear regression model is $\hat{y} = X\hat{\beta}$ where the estimated model parameters $\hat{\beta}$ are

$$\hat{\beta} = (X^T W X)^{-1} X^T W y, \tag{19}$$

where $W$ is a diagonal weight matrix. Here, we set the $j$th component of $W$ to $w_j = \frac{1}{V_j}$ where $V_j$ is the estimated asymptotic variance of $y_i$ determined by the method of LS. Following [30], we form a modified residual

$$r_i = \frac{y_i - \hat{y}_i}{\sqrt{V_i(1 - h_i)}}, \tag{20}$$

where $h_i$ is the i$th$ diagonal element of the hat matrix $H = X(X^T W X)^{-1} X^T W$. This transformation ensures that the modified residuals are realizations of random variables with nearly the same variance. The $i$th component of a bootstrap replication of the observed data is

$$y_i^* = \hat{\beta}_0 + \hat{\beta}_1(t_i - t_1) + \sqrt{V_i} e_i^*, \tag{21}$$

where $i = 1, 2, \cdots 45$ and $(e_1^*, e_2^*, \cdots e_{45}^*)$ is sampled with replacement from $(r_1 - \bar{r}, r_2 - \bar{r}, \cdots r_{45} - \bar{r})$ where $\bar{r}$ is the mean modified residual. From each of 50 000 bootstrap replications of the observed data, we determine a slope and intercept parameter. The bootstrap estimate of the uncertainty of the slope and intercept parameters are the estimated standard deviations of the slope and intercept parameters determined from these estimates.

## 7. Appendix 2: Summary of model selection and uncertainty quantification method

1. Based on a calibration data estimate of $a_{0,\text{calc}}$ for each run, correct $S_{\text{R,obs}}$ spectra per Eq. 8.

2. Set fitting bandwidth to $f_{\text{max}}$ = 200 kHz.

3. Set resampling counter to $n_{\text{resamp}} = 1$.

4. Randomly split $S_{\text{R},cor}$ and $S_{\text{Q,obs}}$ spectral pairs from each of 45 runs into five subsets. Select $d$ by five-fold cross-validation and update appropriate model selection fraction estimate.

5. Increase $n_{\text{resamp}}$ by 1.

6. If $n_{\text{resamp}} < 20\,000$, go to 4.

7. If $n_{\text{resamp}} = 20\,000$, select the polynomial model with largest associated selection fraction. Calculate estimate of residual offset and its uncertainty $\hat{\sigma}_{\text{tot,final}}$ (Eq. 16) from pooled uncorrected spectrum (see Eq. 6).

8. Increase $f_{\text{max}}$ by 25 kHz and go to 3 if $f_{\text{max}} < 1400$ kHz.

9. Select $f_{\text{max}}$ by minimizing $\hat{\sigma}_{\text{tot}}$. Denote the minimum value as $\hat{\sigma}_{\text{tot},*}$.

10. Assign component of uncertainty associated with imperfect performance of method to select $f_{\text{max}}$ as $\hat{\sigma}_{f_{\text{max}}}$ to estimated standard deviation of offset estimates corresponding to $f_{\text{max}}$ values that yield the five lowest values of $\hat{\sigma}_{\text{tot}}$. Our final estimate of the uncertainty of the offset is $\hat{\sigma}_{\text{tot,final}} = \sqrt{\hat{\sigma^2}_{\text{tot},*} + \hat{\sigma^2}_{f_{\text{max}}}}$.

For completeness, we note that simulations and analyses were done with software scripts developed in the public domain R [32] language and environment. Please contact Kevin Coakley regarding any software-related questions.

## 8. References


[1] Moldover M R, Trusler J P M, Edwards T J, Mehl J B and Davis R S (1988). Measurement of the universal gas constant using a spherical acoustic resonator, *J. Res. Natl. Bur. Stand.* 93 85-144.

[2] Pitre L, Sparasci F, Truong D, Guillou A, Risegari L, and Himbert M E (2011). Determination of the Boltzmann constant using a quasi-spherical acoustic resonator, *Int. J. Thermophys.*, vol. 32, pp. 1825-1886.

[3] de Podesta M, R. Underwood G. Sutton, P. Morantz, P. Harris, D.F. Mark, F.M. Stuart, G. Vargha, G. Machin (2013). A low-uncertainty measurement of the Boltzmann constant, *Metrologia*, 50 354-76

[4] Gavioso R M, Benedetto G, Albo P A G, Ripa D M, Merlone A, Guianvarc'h C, Moro F and Cuccaro R (2010). A determination of the Boltzmann constant from speed of sound measurements in helium at a single thermodynamic state, *Metrologia* 47 387-409

[5] Lin H, Feng X J, Gillis K A, Moldover M R, Zhang J T, Sun J P, Duan Y Y (2013). Improved determination of the Boltzmann constant using a single, fixed-length cylindrical cavity, *Metrologia* 50 417-32.

[6] Gaiser C, Zandt T, Fellmuth B, Fischer J, Gaiser C, Jusko O, Priruenrom T,and Sabuga W and Zandt T (2011). Improved determination of the Boltzmann constant by dielectric-constant gas thermometry, *Metrologia* vol. 48, pp. 382-390L7-L11.

[7] Gaiser C, and Fellmuth B (2012). Low-temperature determination of the Boltzmann constant by dielectric-constant gas thermometry, *Metrologia* vol. 49, pp. L4-L7

[8] Benz S P, White D R, Qu J, Rogalla H and Tew W L (2009) Electronic measurement of the Boltzmann constant with a quantum-voltage-calibrated Johnson-noise thermometer, *C. R. Physique.* 10 849858.

[9] Benz S P, Pollarolo A, Qu J F, H Rogalla, Urano C, Tew W L, Dresselhaus P D, and White D R (2011) An electronic measurement of the Boltzmann constant, *Metrologia* vol. 48, pp. 142-153.

[10] Jifeng, Q, S. Benz, A. Pollarolo, H. Rogalla, W. Tew, D. White and K. Zhou, (2015). Improved electronic measurement of the Boltzmann constant by Johnson noise thermometry, *Metrologia*, vol. 52, pp. S242-S256.

[11] Bord, C J (2002), Atomic clocks and inertial sensors *Metrologia 39* pp. 435463/

[12] Fasci, E, M.D. De Vizia, A.Merlone, L.Moretti, A.Castrillo and L.Gianfrani (2015), The Boltzmann constant from the $H_2{}^{18}O$ vibrationrotation spectrum: complementary tests and revised uncertainty budget *Metrologia 52* S233S241.

[13] Kamper R.A. (1972), Survey of noise thermometry, *Temperature, its measurement and control in science and industry, Instrument Society of America, 4*, pp. 349-354.

[14] Blalock T.V. and R.L. Shepard (1982), A decade of progress in high temperature Johnson noise therometry, *Temperature, its measurement and control in science and industry, 5, Instrument Society of America,* pp. 1219-1223.

[15] White D.R., R. Galleano, A. Actis, H. Brixy, M. de Groot, J. Dubbeldam, A Reesink, F. Edler, H. Sakurai, R.L. Shepard, J.C. Gallop (1996), The status of Johnson noise thermometry, *Metrologia 33* pp. 325-335.

[16] Akaike, H. (1973), Information theory and an extension of the maximum likelihood principle In *Second International Symposium on Information Theory,*(eds. B.N. Petrov and F. Czaki) Akademiai Kiado, Budapest, 267-81. 2010

[17] Schwartz, G. (1978), Estimating the dimension of a model *Ann. Statistic. 9*, 130-134.

[18] Mallows, C.(1973), Some comments on $C_p$, *Technometrics 15*, 661-675.

[19] Stone C (1974) Cross-validatory choice and assessment of statistical predictions, *Journal of the Royal Statistical Society. Series B (Methodological)*, *36*(2), pp. 111-147.

[20] Stone C (1977) An Asymptotic Equivalence of Choice of Model by Cross-Validation and Akaike's Criterion, *Journal of the Royal Statistical Society. Series B (Methodological)*, *39*(1) pp. 44-47.

[21] Arlot S. and A. Celisse (2010) A survey of cross-validation procedures for model selection, *Statistical Surveys*, *4*, pp. 40-79

[22] Hastie T., R. Tibshirani and J.H. Friedman (2008) *The Elements of Statistical Learning*, (2nd edition) Springer-Verlag, 763 pages.

[23] Burnham, K.P and D.R. Anderson (2002) *Model Selection and Multimodel Inference: A Practical Information-Theoretical Approach*, 2nd ed., Springer-Verlag, New York

[24] Claeskens, G. and N.L Hjort (2008) *Model Selection and Model Averaging* Cambridge University Press, New York

[25] Picard, R.R. and R.D. Cook (2004), Cross-validation of regression models, *Journal of the American Statistical Association*, Volume 79, pp. 575-583.

[26] Shao, J. (1993) Linear model selection by cross-validation, *Journal of the American Statistical Association 88* pp. 486-494.

[27] Xu, Q.S., Y.Z. Liang and Y.P. Zu, (2004) Monte Carlo cross-validation for selecting a model and estimating the prediction error in multivariate calibration *Journal of Chemometrics 18* pp. 112-120.

[28] B. Efron (2014) Estimation and accuracy after model selection. *Journal of the American Statistical Association*, Volume 109, Issue 507

[29] Efron, B. and R.J. Tibshirani (1993), *An Introduction to the Bootstrap*, Monographs and Statistics and Applied Probability 57, CRC Press

[30] Davison and Hinkley (1997), *Bootstrap Methods and Their Applications*, Cambridge University Press, Cambridge.

[31] Breusch T.S. andd A.R. Pagan (1979), A simple test for heteroscedasticity and random coefficient variation, *Econometrica*, *47*, pp. 1287-1294

[32] R Core Team (2015), R: A language and environment for statistical computing. R Foundation for Statistical Computing, Vienna, Austria. URL https://www.R-project.org/.

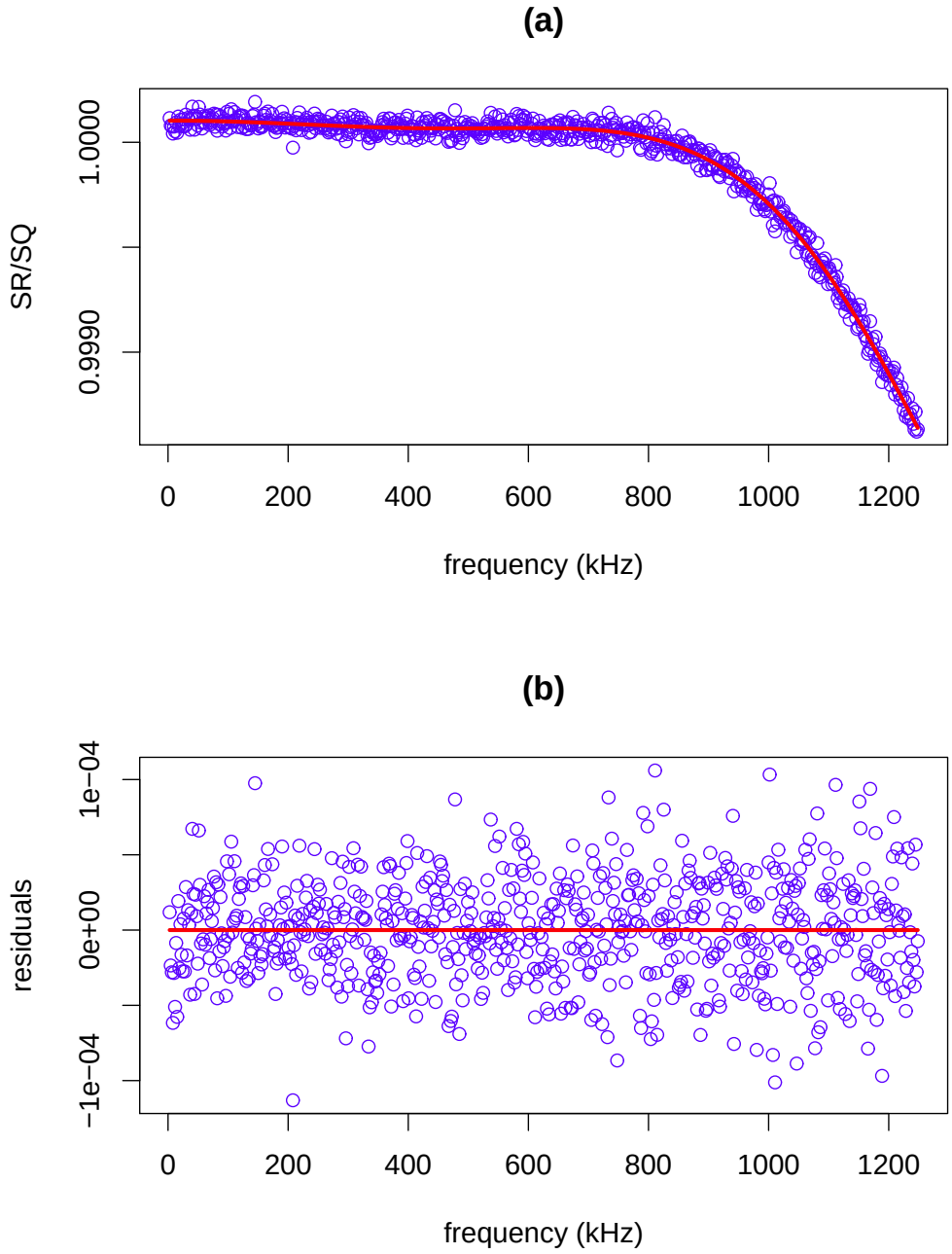


**Figure 1.** Experimental data. (a) Observed (Eq. 6) and predicted ratio spectra based on selected model ($d$=8) and fitting bandwidth (1250 kHz) (see Table 3). (b) Residuals (observed - predicted).

| $f_{\max}$ (kHz) | selection fractions: $p(d)$ $d$=2 | $d$=4 | $d$=6 | $d$=8 | $d$=10 | $d$=12 | $d$=14 |
|---|---|---|---|---|---|---|---|
| 200 | 0.7789 | 0.1269 | 0.0698 | 0.0046 | 0.0159 | 0.0039 | 0.0000 |
| 300 | 0.3271 | 0.2510 | 0.0000 | 0.4160 | 0.0047 | 0.0012 | 0.0000 |
| 400 | 0.0304 | 0.2234 | 0.6427 | 0.0017 | 0.0240 | 0.0716 | 0.0061 |
| 500 | 0.0249 | 0.6043 | 0.0010 | 0.2648 | 0.0701 | 0.0001 | 0.0349 |
| 525 | 0.1347 | 0.0960 | 0.0150 | 0.6758 | 0.0747 | 0.0037 | 0.0000 |
| 550 | 0.0290 | 0.7016 | 0.0000 | 0.0000 | 0.2668 | 0.0027 | 0.0000 |
| 575 | 0.0000 | 0.9446 | 0.0000 | 0.0000 | 0.0012 | 0.0513 | 0.0029 |
| 600 | 0.0000 | 0.9264 | 0.0003 | 0.0000 | 0.0002 | 0.0730 | 0.0000 |
| 625 | 0.0027 | 0.2192 | 0.1273 | 0.0746 | 0.0002 | 0.5289 | 0.0472 |
| 650 | 0.1072 | 0.0022 | 0.2342 | 0.1557 | 0.0006 | 0.0000 | 0.5001 |
| 675 | 0.0320 | 0.0287 | 0.6831 | 0.0077 | 0.0201 | 0.0000 | 0.2285 |
| 700 | 0.2659 | 0.0106 | 0.5514 | 0.0002 | 0.1718 | 0.0000 | 0.0002 |
| 725 | 0.0326 | 0.0181 | 0.8166 | 0.0159 | 0.1067 | 0.0101 | 0.0000 |
| 750 | 0.0700 | 0.0103 | 0.5985 | 0.1475 | 0.0242 | 0.1495 | 0.0001 |
| 775 | 0.0000 | 0.0863 | 0.2889 | 0.3968 | 0.1279 | 0.0980 | 0.0021 |
| 800 | 0.0000 | 0.0216 | 0.4607 | 0.4439 | 0.0017 | 0.0600 | 0.0120 |
| 825 | 0.0009 | 0.0667 | 0.8472 | 0.0320 | 0.0004 | 0.0168 | 0.0362 |
| 850 | 0.0000 | 0.0000 | 0.9294 | 0.0071 | 0.0034 | 0.0059 | 0.0541 |
| 875 | 0.0000 | 0.0000 | 0.8301 | 0.0344 | 0.0001 | 0.0000 | 0.1354 |
| 900 | 0.0278 | 0.0012 | 0.9357 | 0.0314 | 0.0030 | 0.0000 | 0.0009 |
| 925 | 0.0178 | 0.0002 | 0.6384 | 0.3411 | 0.0003 | 0.0000 | 0.0022 |
| 950 | 0.1015 | 0.0000 | 0.0135 | 0.8824 | 0.0022 | 0.0006 | 0.0000 |
| 975 | 0.0421 | 0.0212 | 0.0782 | 0.8560 | 0.0026 | 0.0000 | 0.0000 |
| 1000 | 0.0000 | 0.1072 | 0.1866 | 0.6441 | 0.0622 | 0.0000 | 0.0000 |
| 1025 | 0.0000 | 0.1704 | 0.0000 | 0.8158 | 0.0074 | 0.0029 | 0.0035 |
| 1050 | 0.0010 | 0.0000 | 0.0000 | 0.9751 | 0.0232 | 0.0007 | 0.0000 |
| 1075 | 0.0117 | 0.0001 | 0.0000 | 0.9646 | 0.0235 | 0.0000 | 0.0000 |
| 1100 | 0.0000 | 0.0021 | 0.0000 | 0.9976 | 0.0003 | 0.0000 | 0.0000 |
| 1125 | 0.0000 | 0.0000 | 0.0000 | 0.9519 | 0.0481 | 0.0000 | 0.0000 |
| 1150 | 0.0000 | 0.0000 | 0.0000 | 0.9962 | 0.0012 | 0.0016 | 0.0010 |
| 1175 | 0.0000 | 0.0000 | 0.0000 | 0.9996 | 0.0000 | 0.0003 | 0.0000 |
| 1200 | 0.0000 | 0.0002 | 0.0000 | 0.7125 | 0.1578 | 0.1269 | 0.0027 |
| 1225 | 0.0000 | 0.0000 | 0.0000 | 0.9998 | 0.0002 | 0.0000 | 0.0000 |
| 1250 | 0.0000 | 0.0000 | 0.0000 | 0.9427 | 0.0571 | 0.0003 | 0.0000 |
| 1275 | 0.0000 | 0.0000 | 0.0000 | 0.4784 | 0.5181 | 0.0034 | 0.0000 |
| 1300 | 0.0000 | 0.0000 | 0.0000 | 0.1782 | 0.5986 | 0.2231 | 0.0000 |
| 1325 | 0.0000 | 0.0000 | 0.0000 | 0.0010 | 0.1050 | 0.8885 | 0.0055 |
| 1350 | 0.1879 | 0.2538 | 0.0000 | 0.0000 | 0.0000 | 0.2315 | 0.3268 |
| 1375 | 0.0362 | 0.0322 | 0.0000 | 0.0000 | 0.1788 | 0.7038 | 0.0491 |
| 1400 | 0.2812 | 0.0593 | 0.0000 | 0.0000 | 0.4527 | 0.0060 | 0.2007 |

**Table 1.** Moodel selection fractions for polynomial models for experimental data.

| $f_{\max}$ | $d$ | $\hat{a}_0 - \hat{\bar{a}}_{0,\text{calc}}$ | $\hat{\sigma}_{\hat{a}_0(d),\text{ran}}$ | $\hat{\bar{a}}_0 - \hat{\bar{a}}_{0,\text{calc}}$ | $\tilde{\sigma}_\alpha$ | $\tilde{\sigma}_\beta$ | $\hat{\sigma}_{\text{tot}}$ |
|---|---|---|---|---|---|---|---|
| (kHz) | | $\times 10^6$ | $\times 10^6$ | $\times 10^6$ | $\times 10^6$ | $\times 10^6$ | $\times 10^6$ |
| 200 | 2 | -0.57 | 4.15 | -1.97 | 4.57 | 3.173 | 5.564 |
| 300 | 8 | -7.58 | 5.62 | -2.71 | 4.67 | 4.348 | 6.380 |
| 400 | 6 | -2.09 | 4.40 | -1.35 | 4.41 | 3.041 | 5.357 |
| 500 | 4 | 1.88 | 3.47 | 0.39 | 4.00 | 2.133 | 4.535 |
| 525 | 8 | -0.42 | 4.38 | -0.75 | 4.13 | 1.255 | 4.319 |
| 550 | 4 | 1.90 | 3.26 | 0.51 | 3.69 | 2.179 | 4.290 |
| 575 | 4 | 1.81 | 3.18 | 1.48 | 3.31 | 1.360 | 3.579 |
| 600 | 4 | 2.21 | 3.14 | 1.79 | 3.30 | 1.473 | 3.618 |
| 625 | 12 | -2.65 | 4.83 | -1.04 | 4.31 | 2.295 | 4.886 |
| 650 | 14 | -5.09 | 5.05 | -2.35 | 4.34 | 4.384 | 6.167 |
| 675 | 6 | 3.55 | 3.49 | 1.36 | 3.88 | 3.455 | 5.197 |
| 700 | 6 | 2.88 | 3.40 | -0.95 | 3.32 | 5.318 | 6.271 |
| 725 | 6 | 2.63 | 3.37 | 1.92 | 3.46 | 2.345 | 4.177 |
| 750 | 6 | 1.99 | 3.39 | 0.97 | 3.61 | 3.270 | 4.874 |
| 775 | 8 | 3.88 | 3.72 | 1.78 | 3.68 | 2.422 | 4.404 |
| 800 | 6 | 1.15 | 3.29 | 1.96 | 3.57 | 1.699 | 3.953 |
| 825 | 6 | 1.64 | 3.31 | 0.92 | 3.39 | 2.454 | 4.182 |
| 850 | 6 | 1.61 | 3.25 | 1.50 | 3.36 | 0.545 | 3.403 |
| 875 | 6 | 1.29 | 3.21 | 1.07 | 3.45 | 0.735 | 3.530 |
| 900 | 6 | 1.44 | 3.17 | 1.36 | 3.17 | 0.769 | 3.266 |
| 925 | 6 | 1.03 | 3.13 | 1.49 | 3.27 | 0.656 | 3.334 |
| 950 | 8 | 2.85 | 3.51 | 3.12 | 3.44 | 0.994 | 3.577 |
| 975 | 8 | 2.35 | 3.44 | 2.04 | 3.39 | 4.020 | 5.261 |
| 1000 | 8 | 1.97 | 3.41 | -1.29 | 3.33 | 8.390 | 9.028 |
| 1025 | 8 | 2.73 | 3.44 | -2.49 | 3.41 | 11.510 | 12.010 |
| 1050 | 8 | 2.90 | 3.40 | 2.91 | 3.41 | 0.968 | 3.549 |
| 1075 | 8 | 2.94 | 3.37 | 3.38 | 3.40 | 4.185 | 5.394 |
| 1100 | 8 | 2.78 | 3.37 | 2.69 | 3.37 | 1.842 | 3.837 |
| 1125 | 8 | 3.13 | 3.34 | 3.09 | 3.36 | 0.343 | 3.372 |
| 1150 | 8 | 2.69 | 3.30 | 2.69 | 3.30 | 0.329 | 3.315 |
| 1175 | 8 | 2.82 | 3.30 | 2.82 | 3.30 | 0.012 | 3.301 |
| 1200 | 8 | 2.18 | 3.28 | 2.34 | 3.42 | 0.780 | 3.511 |
| 1225 | 8 | 2.62 | 3.25 | 2.62 | 3.25 | 0.002 | 3.253 |
| 1250 | 8 | 2.36 | 3.22 | 2.40 | 3.24 | 0.145 | 3.246 |
| 1275 | 10 | 3.13 | 3.53 | 2.56 | 3.38 | 0.592 | 3.431 |
| 1300 | 10 | 3.52 | 3.48 | 2.88 | 3.49 | 0.863 | 3.597 |
| 1325 | 12 | 2.23 | 3.76 | 2.42 | 3.73 | 0.553 | 3.774 |
| 1350 | 14 | 3.38 | 4.05 | 25.47 | 6.62 | 90.27 | 90.52 |
| 1375 | 12 | 2.82 | 3.81 | 9.22 | 4.54 | 43.23 | 43.47 |
| 1400 | 10 | 4.32 | 3.57 | 68.13 | 8.41 | 112.2 | 112.5 |

**Table 2.** Results for experimental data.

| parameter | estimate |
|---|---|
| $a_0 - \bar{a}_{0,\text{calc}}$ | 2.36 (3.22) $\times 10^{-6}$ |
| $a_2$ | -4.33 (0.41) $\times 10^{-4}$ |
| $a_4$ | 1.66 (0.13) $\times 10^{-3}$ |
| $a_6$ | -2.25 (0.13) $\times 10^{-3}$ |
| $a_8$ | 6.26 (0.46) $\times 10^{-4}$ |

**Table 3.** Estimated model parameters for experimental data for $f_{\text{max}} = 1250$ kHz.

| | $f_{\text{max}}$ (kHz) | $d$ | $\hat{a}_0 - \hat{\bar{a}}_{0,\text{calc}}$ $\times 10^6$ | $\hat{\sigma}_{\hat{a}0(d),\text{ran}}$ $\times 10^6$ | $\hat{\bar{a}}_0 - \hat{\bar{a}}_{0,\text{calc}}$ $\times 10^6$ | $\tilde{\sigma}_\alpha$ $\times 10^6$ | $\tilde{\sigma}_\beta$ $\times 10^6$ | $\hat{\sigma}_{\text{tot},*}$ $\times 10^6$ | $\hat{\sigma}_{f_{\text{max}}}$ $\times 10^6$ | $\hat{\sigma}_{\text{tot,final}}$ $\times 10^6$ |
|---|---|---|---|---|---|---|---|---|---|---|
| experimental | 1250 | 8 | 2.36 | 3.22 | 2.40 | 3.24 | 0.14 | 3.25 | 0.56 | 3.29 |
| realization 1 | 1400 | 8 | 4.25 | 2.64 | 4.20 | 2.66 | 0.18 | 2.67 | 0.39 | 2.69 |
| realization 2 | 1150 | 8 | -0.43 | 2.98 | -0.39 | 3.00 | 0.59 | 3.05 | 0.45 | 3.08 |
| realization 3 | 1325 | 8 | -2.59 | 2.76 | -2.88 | 2.82 | 0.60 | 2.89 | 1.83 | 3.42 |

**Table 4.** Comparison of selected $f_{\text{max}}$ and associated model parameters for experimental and simulated data sets. In the simulation, the true values of $a_0 - a_{0,\text{calc}}$ and $d$ are 0 and 8 respectively. The component of uncertainty $\hat{\sigma}_{f_{\text{max}}}$ accounts for imperfect performance of our $f_{\text{max}}$ selection method.

| $f_{\max}$ (kHz) | $d$ | intercept $\times 10^6$ | slope $\times 10^6$ day | $p$-value (trend test) | $\chi^2_{\text{obs}}$ | $p$-value (model consistency test) | $a_0 - \bar{a}_{0,\text{calc}}$ $\times 10^6$ |
|---|---|---|---|---|---|---|---|
| 200 | 2 | 11.98(6.50) | -0.243(0.125) | 0.050 | 33.0 | 0.864 | -0.57(5.56) |
| 300 | 8 | 11.74(10.54) | -0.440(0.199) | 0.027 | 47.0 | 0.311 | -7.58(6.38) |
| 400 | 6 | 10.31(6.64) | -0.247(0.126) | 0.062 | 35.8 | 0.775 | -2.09(5.36) |
| 500 | 4 | 10.69(5.12) | -0.175(0.097) | 0.072 | 32.6 | 0.877 | 1.88(4.54) |
| 575 | 4 | 10.13 (4.42) | -0.164 (0.084) | 0.049 | 28.2 | 0.960 | 1.81(3.58) |
| 700 | 6 | 13.56(4.95) | -0.213(0.093) | 0.021 | 31.0 | 0.914 | 2.88(6.27) |
| 800 | 6 | 10.49(3.94) | -0.175(0.074) | 0.018 | 22.5 | 0.996 | 1.15(3.95) |
| 900 | 6 | 9.15 (3.49) | -0.164 (0.066) | 0.012 | 19.9 | 0.999 | 1.44(3.27) |
| 1150 | 8 | 11.39 (3.79) | -0.179 (0.071) | 0.011 | 23.2 | 0.994 | 2.69(3.32) |
| 1175 | 8 | 11.57 (3.81) | -0.185 (0.072) | 0.010 | 24.0 | 0.991 | 2.82(3.30) |
| 1225 | 8 | 12.13 (3.79) | -0.204 (0.071) | 0.004 | 25.0 | 0.987 | 2.62(3.25) |
| 1250 | 8 | 12.02 (3.78) | -0.202 (0.071) | 0.004 | 25.2 | 0.986 | 2.36(3.25) |

**Table 5.** Estimated trend model parameters, associated uncertainties and $p$-values for testing the no-trend hypothesis (column 5). Based on $\chi^2_{\text{obs}}$ and the number of degrees-of-freedom (43), we determine a $p$-value (column 7) for testing the hypothesis that the linear trend model is consistent with observations. The value $f_{\max} = 575$ kHz corresponds to selected fitting bandwidth in [10]. The five values (ranging from 900 kHz to 1250 kHz) yield the five lowest values of $\hat{\sigma}_{\text{tot}}$ when $f_{\max}$ is varied from 200 kHz to 1400 kHz on a grid. For comparison, we list results at fitting bandwidths of 200 kHz, 300 kHz, 400 kHz, 500 kHz, 700 kHz and 800 kHz. In the last column, we list estimates of $a_0 - \bar{a}_{0,\text{calc}}$ from the pooled data and their associated $\hat{\sigma}_{\text{tot}}$ values in parentheses.

(Table 2).

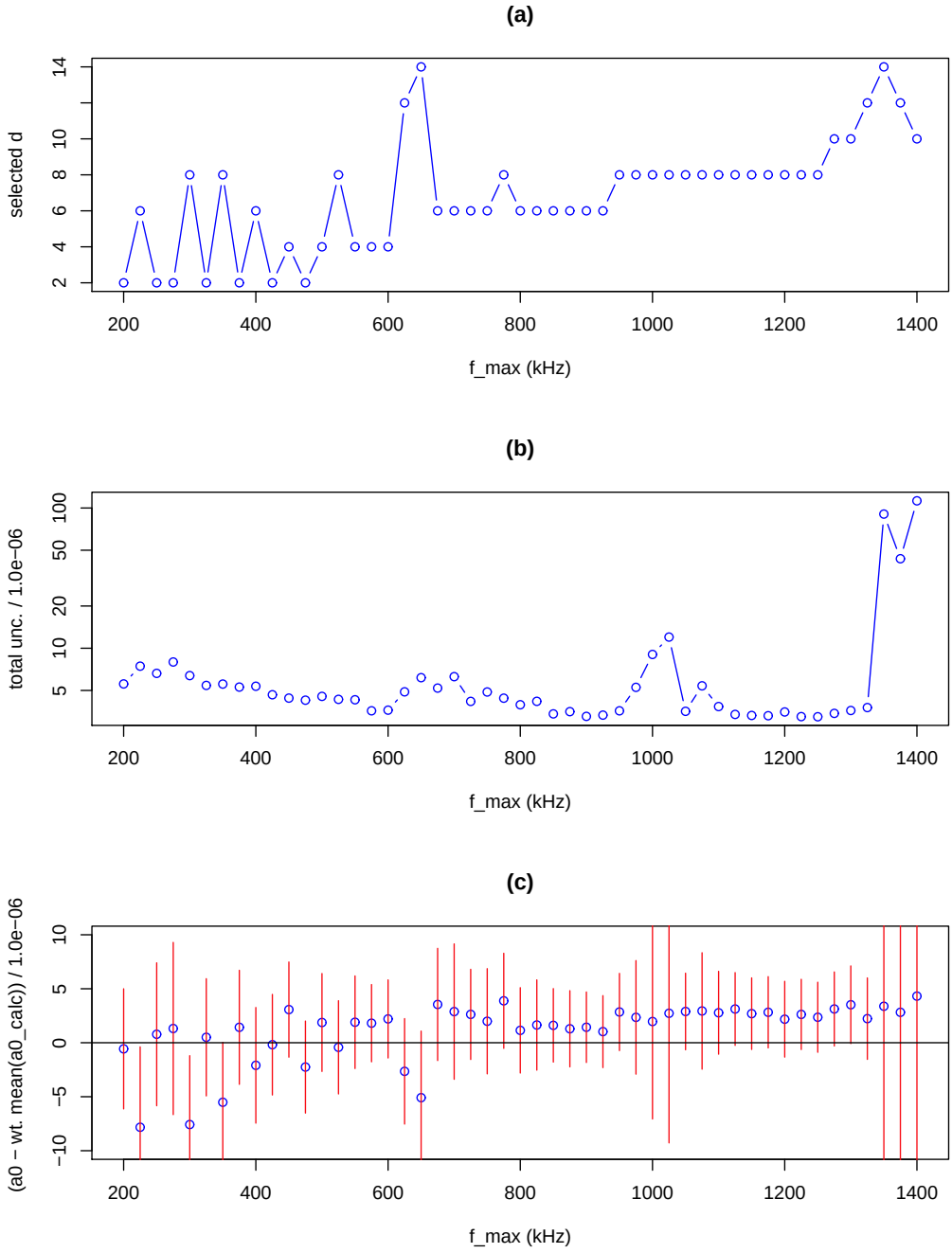


**Figure 2.** Experimental data. (a) Estimated polynomial complexity parameter $d$. (b) Estimated total uncertainty $\hat{\sigma}_{\text{tot}}$ (Eq. 13). (c) Estimated $a_0 - \bar{a}_{0,\text{calc}}$ and approximate 68 % coverage interval.

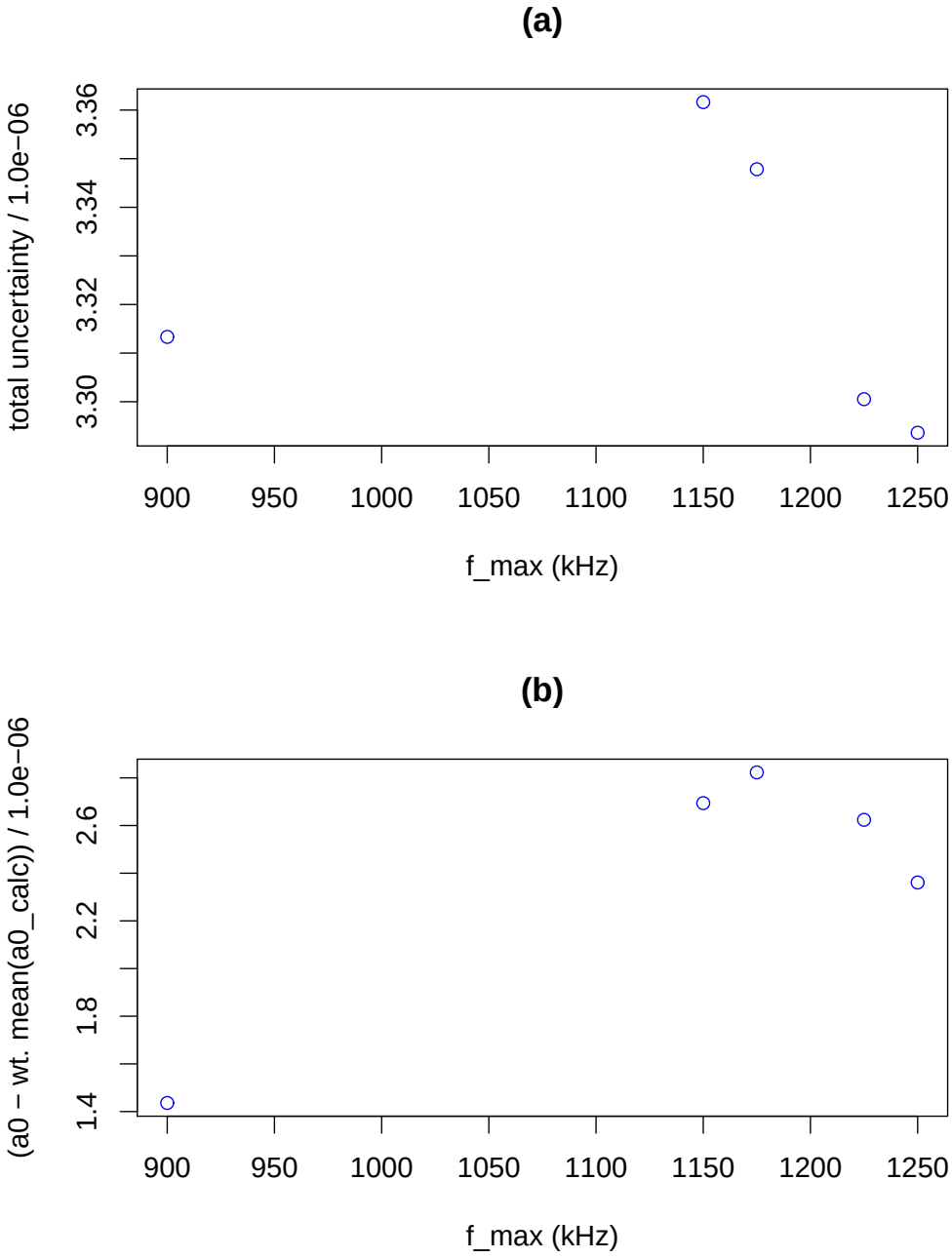


**Figure 3.** Experimental data. Results for $f_{\max}$ values which yield the five lowest values of $\hat{\sigma}_{\text{tot}}$. (a) $\hat{\sigma}_{\text{tot}}$ versus $f_{\max}$. (b) Estimated $a_0 - \bar{a}_{0,\text{calc}}$ versus $f_{\max}$.

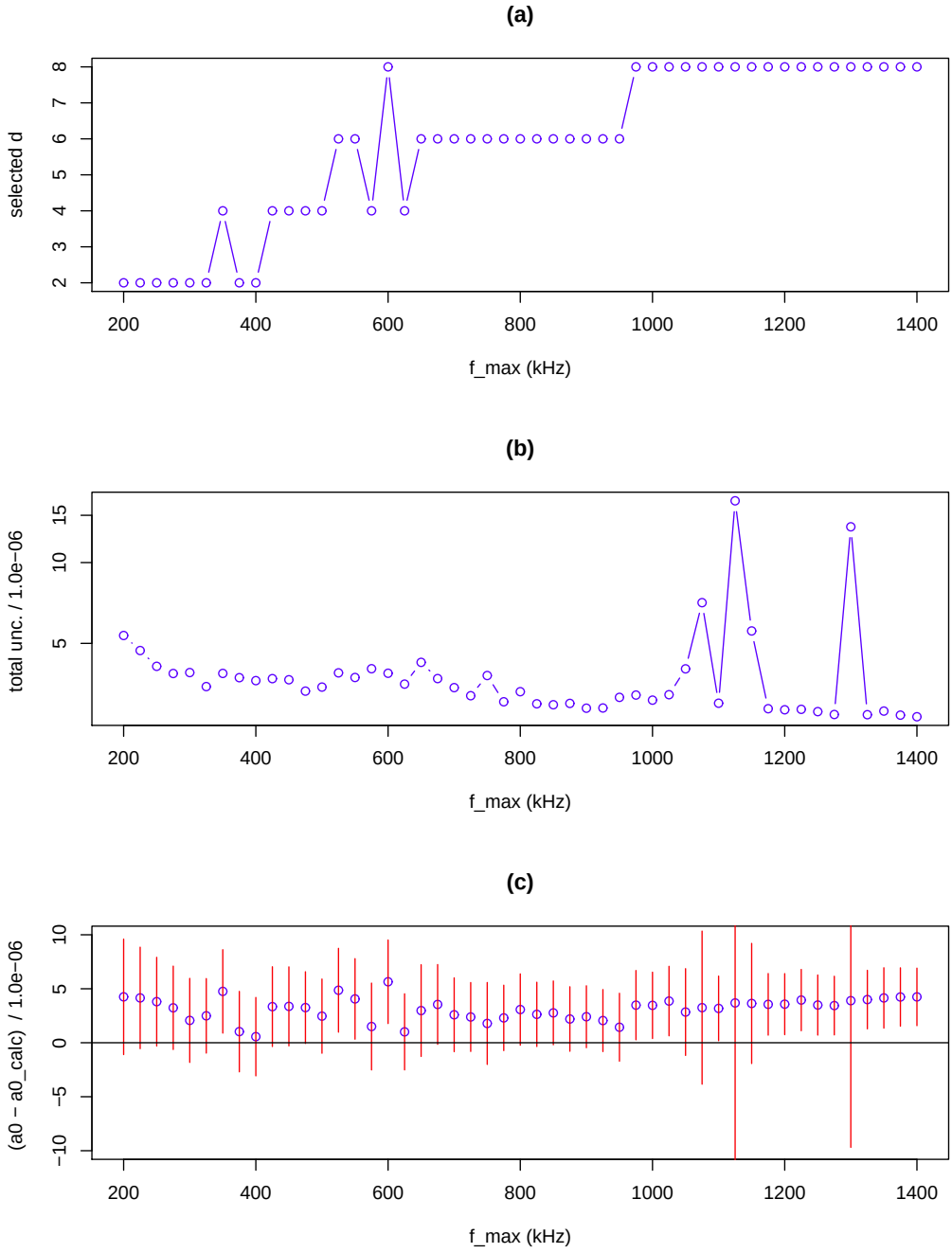


**Figure 4.** Simulated data (realization 1). (a) Estimated polynomial complexity parameter $d$. (b) Estimated total uncertainty $\hat{\sigma}_{\text{tot}}$. (c) Estimated $a_0 - a_{0,\text{calc}}$ and approximate 68 % coverage interval. The true value of $a_0 - a_{0,\text{calc}}$ is 0.

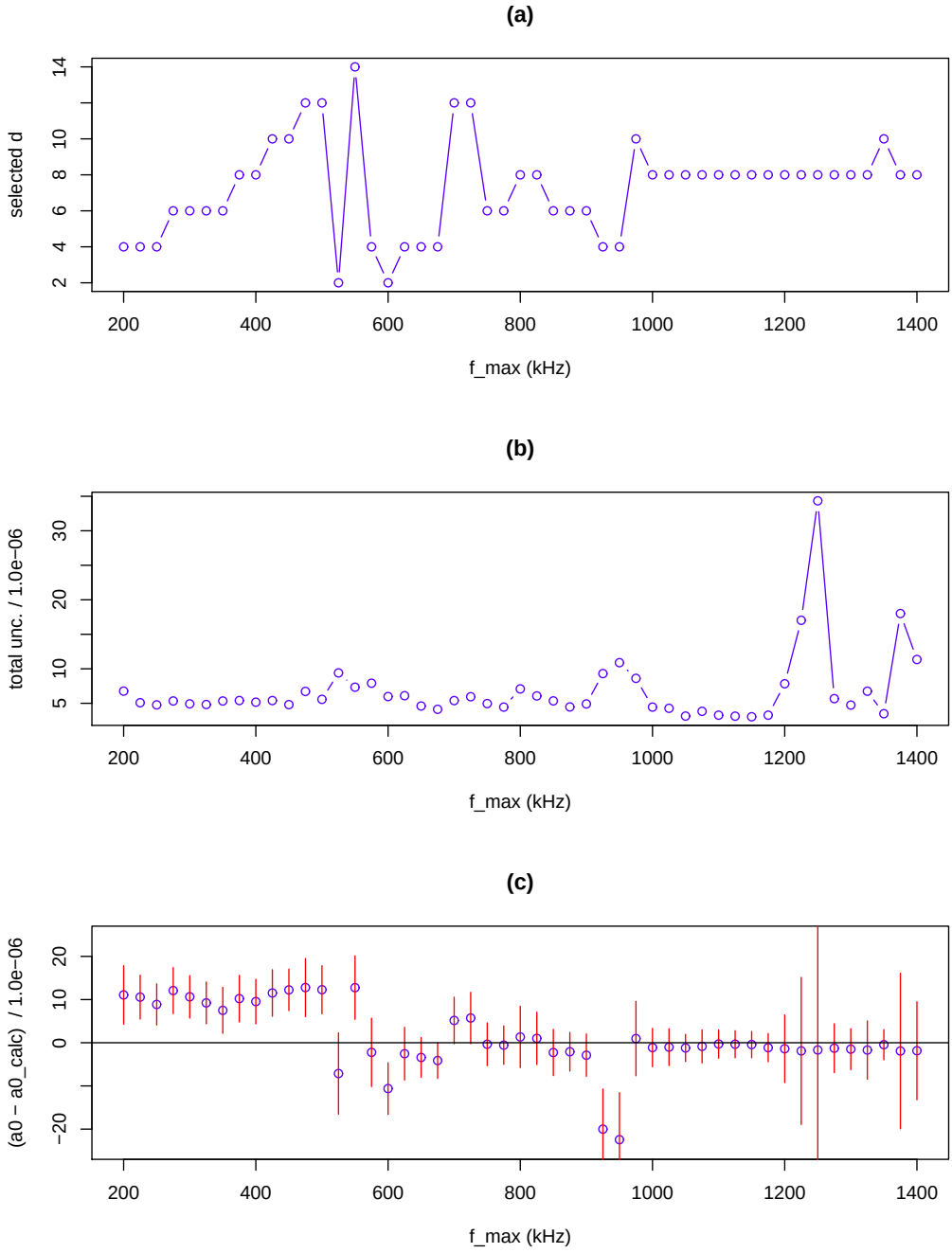


**Figure 5.** Simulated data (realization 2). (a) Estimated polynomial complexity parameter $d$. (b) Estimated total uncertainty $\hat{\sigma}_{\text{tot}}$. (c) Estimated $a_0 - a_{0,\text{calc}}$ and approximate 68 % coverage interval. The true value of $a_0 - a_{0,\text{calc}}$ is 0.

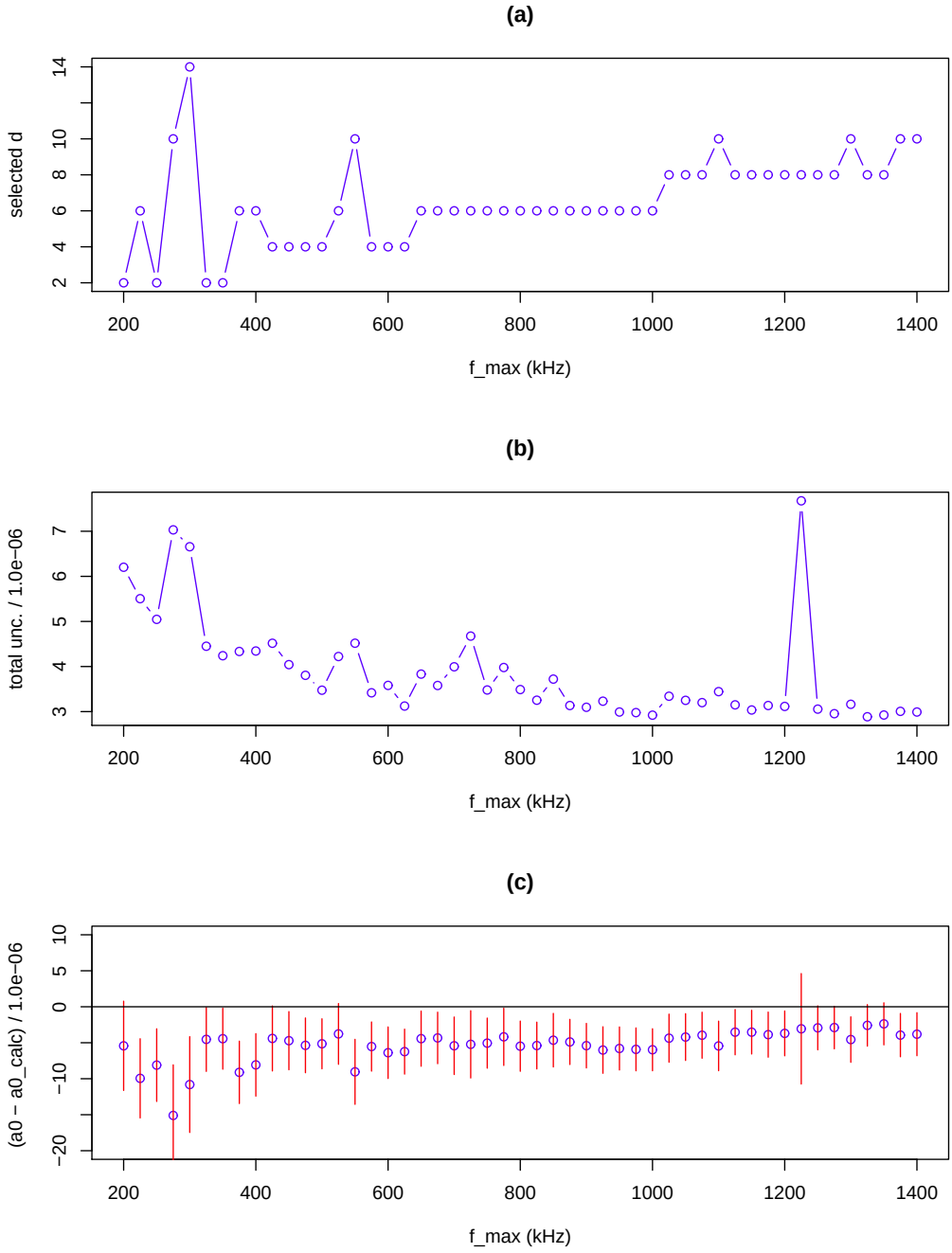


**Figure 6.** Simulated data (realization 3). (a) Estimated polynomial complexity parameter $d$. (b) Estimated total uncertainty $\hat{\sigma}_{\text{tot}}$. (c) Estimated $a_0 - a_{0,\text{calc}}$ and approximate 68 % coverage interval. The true value of $a_0 - a_{0,\text{calc}}$ is 0.

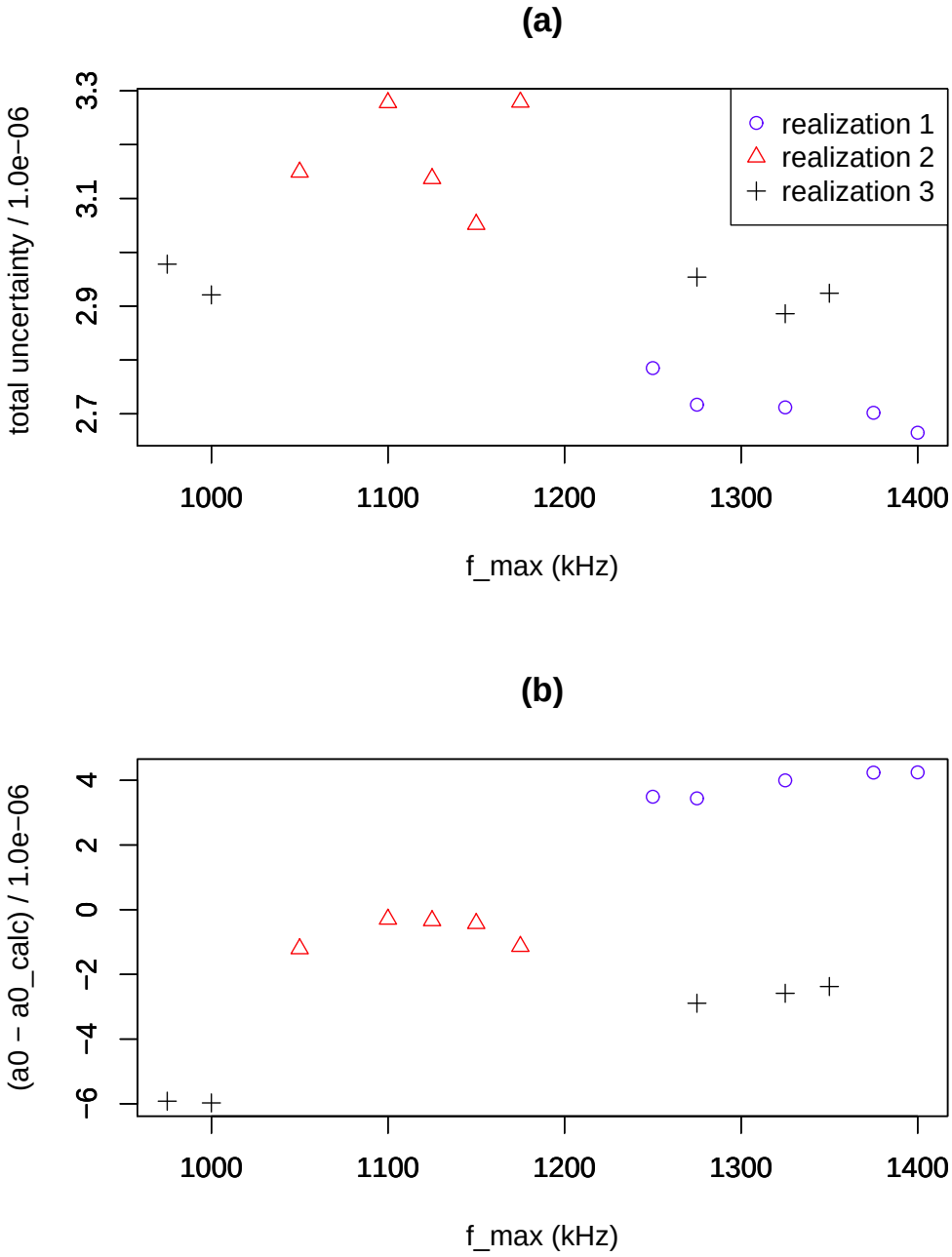


**Figure 7.** Simulated data. Results for $f_{\max}$ values which yield the five lowest values of $\hat{\sigma}_{\text{tot}}$. (a) $\hat{\sigma}_{\text{tot}}$ versus $f_{\max}$. (b) estimated $a_0 - a_{0,\text{calc}}$ versus $f_{\max}$. The true value of $a_0 - a_{0,\text{calc}}$ is 0.

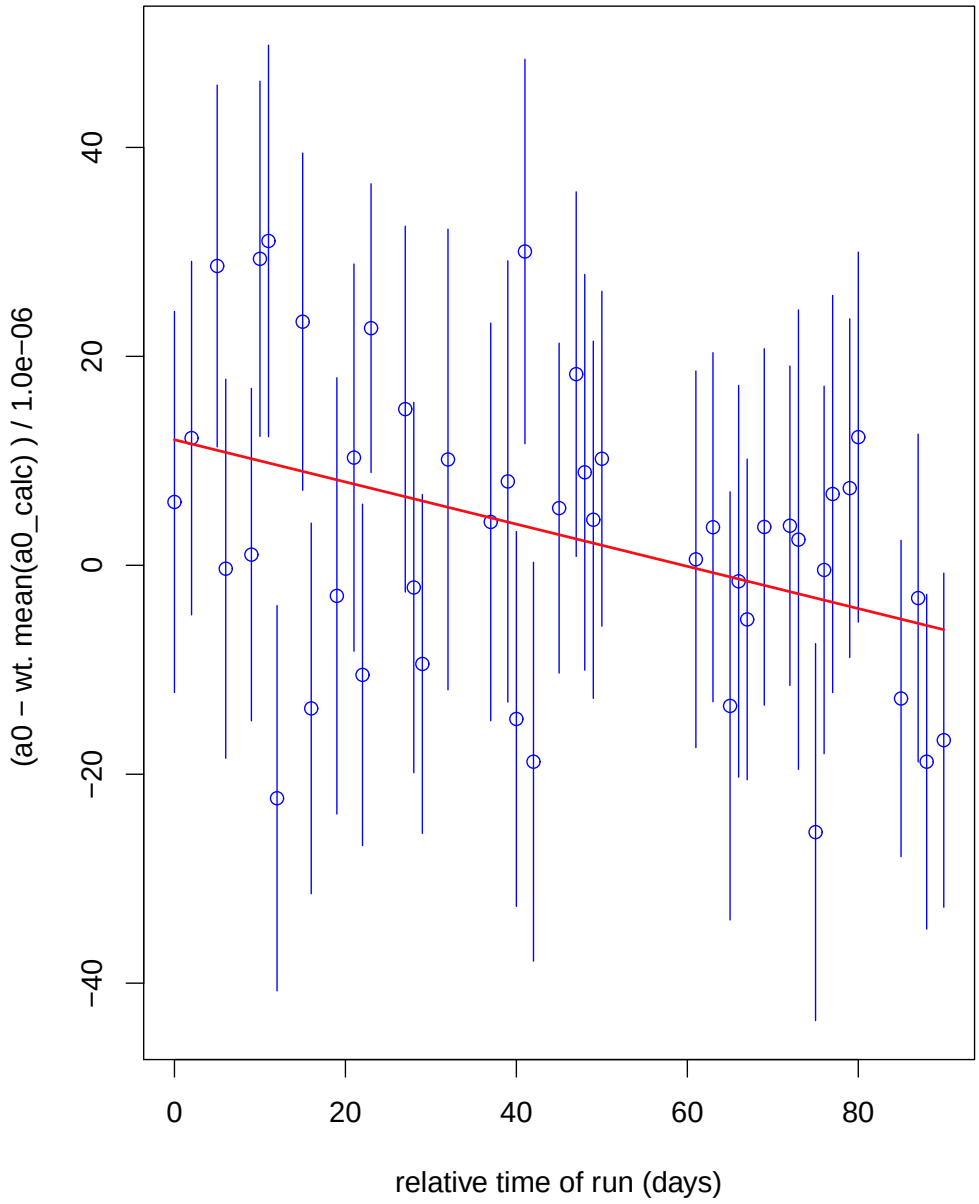


**Figure 8.** From the corrected ratio spectrum (Eq. 7), we estimate $a_0 - \bar{a}_{0,\text{calc}}$ for each run by fitting a $d = 8$ ratio spectrum model by the method of Least Squares. The half-widths of the intervals are asymptotic uncertainties determined by the Least Squares method. The fitting bandwidth is $f_{\text{max}}$ = 1250 kHz.